Bulletin of Electrical Engineering and Informatics
Vol. 15, No. 6, December 2026, pp. 4863∼4875
ISSN: 2302-9285, DOI: 10.11591/eei.v15i6.12383

Photovoltaic-integrated system for electric vehicle charging in single-phase electrical grids

José Manuel Aller, Cristian Fernando León Zhagñay, Bruno Vinicio Ortiz Cárdenas
Department of Electrical Engineering, Universidad Politecnica Salesiana, Cuenca, Ecuador

Article Info

Article history:

Received Jan 22, 2026
Revised Sep 18, 2026
Accepted Oct 4, 2026

Keywords:

Active and reactive power control
ATP–EMTP
Electric vehicle charging
Photovoltaic systems
Single-phase grid-connected inverter

ABSTRACT

This paper presents the modeling and analysis of a photovoltaic (PV)–based electric vehicle (EV) charging system integrated into a single-phase distribution grid. The complete system is implemented in the ATP–EMTP environment using the ATPDraw graphical interface, including PV generation with maximum power point tracking (MPPT)-controlled DC–DC conversion, a single-phase grid-connected inverter with sinusoidal pulse width modulation (SPWM), inductor capacitor inductor (LCL) filtering, and bidirectional power-flow capability. The distinctive contribution of this work is the integration of the complete conversion and control chain within a unified circuit-level ATP–EMTP/ATPDraw framework, while explicitly considering the double-frequency power oscillations inherent to single-phase grid interfaces. Unlike balanced three-phase operation, single-phase systems exhibit power oscillations at twice the grid frequency, which complicates controller tuning and power regulation. Coordinated active- and reactive-power regulation is therefore implemented using synchronized proportional integral (PI) controllers and a phase-locked loop (PLL) represented through ATPDraw MODELS blocks. Simulation results demonstrate stable operation under irradiance variations and effective power regulation. For active-power references of 1–2 kW, representative steady-state tracking errors remain below 0.7%, while the final 1 kW operating interval exhibits an average reactive-power estimate of approximately 21 var.

This is an open access article under the CC BY-SA license.

Corresponding Author:

José Manuel Aller
Department of Electrical Engineering, Universidad Politecnica Salesiana
Cuenca 010105, Ecuador
Email: jaller@ups.edu.ec

1. INTRODUCTION

Grid-connected electric vehicle (EV) charging architectures increasingly consider bidirectional power flow and grid-support capabilities, motivated by concepts such as vehicle-to-grid (V2G), peak shaving, and ancillary services [1]–[3]. Recent studies of single-phase grid-connected converters similarly emphasize the combined role of modulation, filtering, and converter control in limiting harmonic propagation and maintaining power quality [4]–[7]. The present ATP–EMTP implementation reproduces these switching phenomena explicitly at circuit level, allowing their interaction with the remaining photovoltaic (PV)–EV charging system to be examined within the same simulation environment. However, practical deployments in many regions rely predominantly on single-phase distribution networks, which impose additional constraints on inverter design and control.

In particular, unlike balanced three-phase systems—where active and reactive powers can be treated as quasi-constant under steady-state conditions—single-phase interfaces exhibit intrinsic power oscillations at twice the grid frequency. These oscillations complicate the regulation of active and reactive power and require careful synchronization and controller tuning. This behavior has been explicitly identified in single-phase V2G and grid-connected converters, where the pulsating AC-side power produces second-harmonic components that can propagate toward the DC link and affect both dynamic performance and converter reliability [8], [9]. Consequently, several approaches based on adaptive filtering, synchronous-reference-frame control, and dedicated second-harmonic suppression have been proposed to improve power regulation and DC-link behavior [10], [11].

Although these studies demonstrate substantial advances in converter topologies, harmonic mitigation, and active–reactive power control, the different stages of PV-assisted EV charging are frequently analyzed as individual conversion or control subsystems. For system-level studies, there remains practical value in a unified circuit-level framework capable of representing PV generation, maximum power point tracking (MPPT)-controlled DC–DC conversion, inverter switching, grid synchronization, filtering, and power regulation within the same electromagnetic-transients simulation environment. Such a framework is particularly useful for assessing the interaction among these subsystems under the intrinsic time-varying power conditions of a single-phase grid.

Motivated by the Ecuadorian context, where PV integration into EV charging is still emerging, this paper develops a circuit-level PV-based EV charging model suitable for single-phase grids. The system is implemented in ATP–EMTP using the ATPDraw graphical environment, integrating PV generation, MPPT-controlled DC–DC conversion, a single-phase inverter with sinusoidal pulse width modulation (SPWM), inductor capacitor inductor (LCL) filtering, and coordinated control of active and reactive power. The distinctive contribution of the proposed approach is not an individual converter topology or control algorithm, but the integration of these elements into a unified and reproducible circuit-level model in which the dynamic interactions associated with single-phase power regulation can be directly examined. The resulting framework provides a reproducible basis for analyzing dynamic behavior, power-quality performance, and feasibility of PV-integrated EV charging in residential applications.

The main contributions of this paper can be summarized as follows:

a. Development of a unified circuit-level model of a PV-integrated EV charging system for single-phase grids in ATP–EMTP/ATPDraw, including the PV source, MPPT-controlled DC–DC stage, SPWM inverter, LCL filter, grid interface, and charging load.
b. Implementation of coordinated active and reactive power regulation with phase-locked loop (PLL)-based grid synchronization, explicitly considering the double-frequency power oscillations inherent to single-phase operation.
c. Assessment of the interaction among the PV, conversion, filtering, and power-control stages under variable irradiance and grid-connected operating conditions.
d. Evaluation of the technical and economic applicability of the integrated framework to residential and small-scale EV charging supplied from single-phase distribution networks.

2. METHOD

ATPDraw was used for simulating and analyzing the PV-charging system, modeling both transient and steady-state behaviors of renewable generation, inverters, and grid components. The MODELS block enabled custom mathematical and logical relationships, essential for calculating active/reactive power, power factor, and implementing inverter control functions [12], [13].

2.1. Analysis of electric vehicle for charging system sizing

EV specifications in Ecuador were analyzed, including charging power, battery capacity, efficiency, and range. Based on this review, the system was sized to supply approximately 8 kW, ensuring compatibility with most local EV and providing a margin for variations and future models, making it suitable for residential and small commercial applications.

2.2. Inductor capacitor inductor filter

The LCL filter, consisting of two inductors and a capacitor, smooths inverter output and reduces high-frequency harmonics [14], [15]. Simulations in ATPDraw showed attenuation of high-frequency switching

components and stable grid interaction, supporting the technical feasibility of the design. In the simulation, low-pass filters were used to preserve fundamental signal components and attenuate high-frequency harmonics [16], improving measurement accuracy, reducing noise, and enabling reliable dynamic and power quality analysis.

2.3. Sizing of the single-phase inverter

ATPDraw was used to size and evaluate the system, providing accurate simulation of electrical and power electronic circuits with realistic component modeling [17]. The single-phase inverter, the core of the conversion stage, was modeled in ATPDraw using four insulated-gate bipolar transistor (IGBT)-like switches Q_1, Q_2, Q_3, and Q_4 controlled by the MODELS block "TRIG" shown in Figure 1, with diodes and $15\,\mathrm{m\Omega}$ resistors ensuring stable switching and numerical performance.

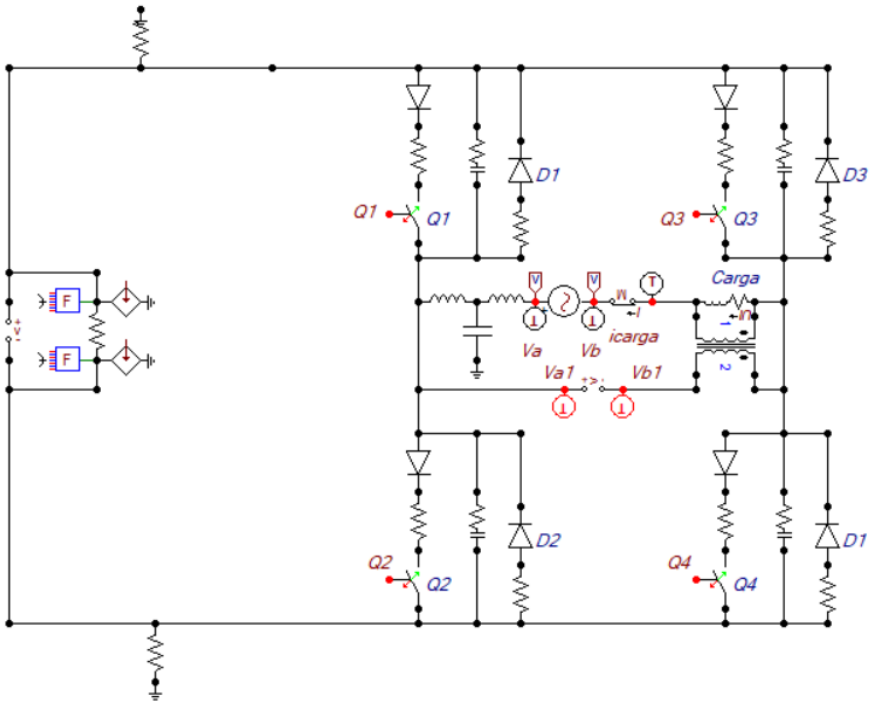


Figure 1. Single phase inverter circuit modeled in ATPDraw

A snubber composed of a $1\,\Omega$ resistor and a 10 nF capacitor protected the inverter switches from transients. Initial tests used a 120 V DC source, which was later replaced by a PV panel model with typical irradiance and temperature values. The load consisted of a 159.79 V AC network, corresponding to an RMS voltage of approximately 120 V, with a series resistance of $5\,\mathrm{m\Omega}$ and an inductance of 50 nH to emulate grid conditions. An LCL filter with an inductance of 1 mH and a capacitance of 50 nF reduced high-frequency harmonics and stabilized the AC output. A 1:1 isolation transformer was included to provide galvanic isolation and electrical coupling between the inverter and the utility grid, while the LCL filter performs the main high-frequency harmonic attenuation.

2.4. Modeling of a photovoltaic panel

The PV model, driven by temperature and irradiance inputs, generates voltage, current, and instantaneous power, which feed the MPPT algorithm to compute the optimal duty cycle. This drives the Boost converter, producing V_{L-rms} and $PV_{neg-rms}$ for stable RMS-based power assessment, enabling evaluation of the boost converter and MPPT performance. The complete system is shown in Figure 2 [17].

2.5. Generation of the triangular waveform using a MODELS block

The triangular waveform is generated using a MODELS block in ATPDraw, where parameters such as frequency, amplitude, and the number of triangles per half-cycle are defined. The model calculates the time

step, advances the waveform, and inverts the slope when the signal reaches its limits. The final output is a triangular signal that synchronizes with the sinusoidal reference, which is then used to create the SPWM signal for triggering the IGBT switches in the inverter.

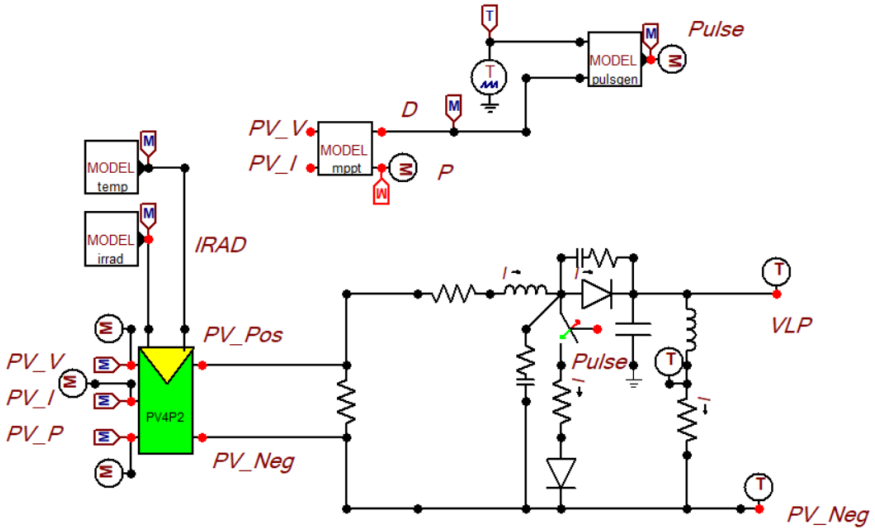


Figure 2. PV panel and DC–DC converter and MPPT algorithm simulated in ATPDraw

2.6. Sinusoidal pulse width modulation modeling using a MODELS block in ATPDraw

The SPWM signal is generated in ATPDraw using a MODELS block that continuously compares a sinusoidal reference with a triangular carrier. Based on this comparison, the model produces a high or low switching signal that follows the sign of the sinusoidal reference. This pulse sequence is used to drive the inverter IGBT switches, shaping the output voltage into a near-sinusoidal waveform with reduced harmonic distortion.

2.7. Active power on the load

The active load power is calculated in ATPDraw using a MODELS block that measures the voltage difference between nodes V_a and V_b and multiplies it by the instantaneous load current. This approach provides an automatic and accurate estimation of the instantaneous active power delivered to the load, enabling effective evaluation of load performance during simulation.

With the load voltage and current known, instantaneous power is calculated using the basic circuit theory relationship,

$$P_{load}(t) = v_{ab}(t)\, i_{load}(t) \tag{1}$$

The instantaneous power defined in (1) enables dynamic energy evaluation and feeds subsequent modules such as average-power filters for system analysis.

2.8. Effective voltage and effective current

The TAC block computes the RMS load current and voltage, providing accurate measurements that help evaluate inverter performance, power delivery, and overall output quality.

2.9. Apparent and reactive power with their corresponding sign

The apparent and reactive power are calculated in ATPDraw using a MODELS block based on RMS voltage and current measurements. The model computes apparent power as the product of RMS voltage and current, while reactive power is obtained from the power triangle using the known active power [18]. The sign of the reactive power is determined from the voltage magnitude and phase relationship, allowing identification of inductive or capacitive behavior and supporting analysis of load characteristics and inverter performance.

In this model, the reactive power Q is calculated from the apparent power and the active power using the expression (2):

$$Q = \text{sgn}\left(V_{inv}\ \cos(\phi_{red}) - V_{ab}\right)\sqrt{S^2 - P^2} \tag{2}$$

In (2) is based on the conventional power-triangle relation $S^2 = P^2 + Q^2$. Consequently, the computed quantity corresponds exactly to reactive power when the voltage and current are approximately sinusoidal. Under distorted conditions, however, $\sqrt{S^2 - P^2}$ represents the magnitude of the non-active power and may include contributions associated with waveform distortion. In the present implementation, this quantity is used as the feedback variable of the reactive-power control loop, while its sign is determined from the relative inverter/grid voltage magnitude and phase relationship [19].

In (2) shows the inverter's voltage phase relative to the grid: if $Q > 0$, the PV inverter supplies reactive power to the grid; if $Q < 0$, the grid provides reactive power to the inverter, which can then deliver it to the vehicle's batteries.

2.10. Phase-locked loop

The PLL is implemented in ATPDraw using a MODELS block that synchronizes the inverter with the grid by tracking the input voltage phase and frequency. The model detects the phase error between the grid voltage and the internal oscillator, processes it through a proportional integral (PI) controller, and adjusts the oscillator frequency accordingly. A voltage-controlled oscillator then updates the angular frequency and phase, generating a synchronized sinusoidal reference used for inverter control, ensuring stable power injection and accurate phase alignment [18].

2.11. Proportional integral controller for active and reactive power

The PI controllers shown in Figure 3 regulate active and reactive power by minimizing the error between reference and measured signals. The proportional term provides immediate response, while the integral term eliminates steady-state error. Gains k_p and k_i were empirically tuned to ensure stable, fast, and accurate power regulation with reliable grid synchronization.

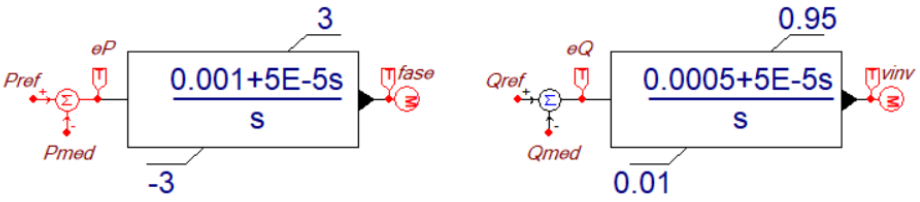


Figure 3. PI controllers for active and reactive power loops

2.12. Fundamental waveform control in amplitude and phase

After tuning the optimal k_p and k_i values, the control loops regulate active and reactive power. Active power follows a time-varying reference simulating realistic load, while reactive power is kept near zero to maintain unity power factor and minimize grid reactive exchange.

As shown in Figure 3, the active-power controller outputs the phase variable, which a MODELS block uses to generate the sinusoidal reference with the proper phase shift. Simultaneously, the reactive-power controller outputs v_{inv} to set the reference waveform's amplitude. Together, these controls regulate both phase and amplitude, ensuring correct active power injection and near-zero reactive power.

The MODELS block generating the sinusoidal reference waveform receives phase $phivco$ and frequency $fvco$ from the PLL, ensuring full grid synchronization. This sinusoid is compared with the triangular-wave carrier to produce the SPWM signal, which drives the inverter switches, enabling controlled active and reactive power exchange under the simulated operating conditions.

2.13. Technical–economic analysis of the project

This subsection evaluates the technical feasibility and economic performance of the proposed PV–based EV charging system under typical residential operating conditions. The system integrates MPPT-controlled DC–DC conversion, a single-phase grid-connected inverter, and coordinated active and reactive power control, enabling flexible interaction between the PV array, the utility grid, and the EV load.

From a regulatory perspective, relevant standards for the proposed application include IEC 61851 for EV charging systems [20], [21], IEEE Std 1547-2018 for distributed energy resource interconnection [22], and IEEE Std 2030.1.1-2021 for DC fast-charging infrastructure [23]. These standards provide a reference framework for grid interconnection and charging infrastructure requirements. The present work, however, is based on circuit-level simulation and should therefore be interpreted as a technical feasibility assessment rather than as a formal certification or compliance test.

Operationally, the simulated system can operate in solar-only, hybrid, and grid-export modes. Its dynamic behavior and control performance were evaluated through ATPDraw simulations, which showed stable operation and effective average power regulation under the investigated conditions. These results support the technical feasibility of the proposed architecture for residential PV-integrated EV charging, while experimental validation remains a subject for future work.

2.13.1. Project cost estimate

The economic assessment considers a residential installation composed of an 8 kW single-phase EV charger supplied by a 6 kW PV system, capable of covering approximately 70% of the annual energy demand. The evaluation includes PV modules, a bidirectional inverter, EV charger, electrical protections, wiring, structural components, installation, and labor.

Three implementation scenarios are analyzed: economy, standard, and professional. These scenarios differ in component quality, certification level, expected lifetime, and installation complexity, allowing a comparative assessment between lower initial investment and long-term system robustness.

Table 1 summarizes the estimated investment required for the three residential implementation scenarios. The PV array represents the largest fraction of the total cost in all cases, followed by the bidirectional inverter and installation expenses. While the economy configuration minimizes the initial investment, the professional alternative prioritizes certified equipment, higher expected lifetime, and greater operational reliability, making it more suitable for long-term residential installations.

Table 1. Estimated investment cost for residential PV–EV charging system

Component	Economy (kUSD)	Standard (kUSD)	Professional (kUSD)
PV array (6 kW)	3.0–4.2	4.8–6.0	7.0–9.0
Bidirectional inverter (5–7 kW)	1.3–1.8	2.0–2.6	3.0–3.5
EV charger (8 kW)	0.5–0.7	0.8–1.1	1.2–1.5
Protections and installation	0.4–0.7	0.7–1.0	1.2–1.5
Wiring and conduits	0.2–0.3	0.3–0.6	0.7–1.0
Labor	0.5–1.0	1.0–1.7	1.8–2.5
Total investment	6.1–9.05	10.0–13.6	15.5–19.9

In addition to the initial investment, maintenance expenditures affect the long-term economic performance of the system. These expenditures include PV panel cleaning, inverter and protection inspection, structural verification, and technical labor. Indicative costs associated with these maintenance activities are summarized in Table 2. Compared with the initial capital investment, the annual maintenance represents a relatively small fraction of the total ownership cost, indicating that the economic viability of the system is primarily influenced by the initial installation cost rather than by routine maintenance expenditures.

Table 2. Indicative maintenance costs for the PV system

Item	Estimated cost (USD)
PV panel cleaning and maintenance	40–120
Inverter and protection inspection	30–80
Structural and wiring inspection	20–60
Technical service and labor	50–150

The economic evaluation assumes an EV traveling approximately 22,000 km per year with an average energy consumption of 0.20 kWh/km, resulting in an annual EV energy demand of 4,400 kWh.

Based on these operating assumptions and the investment and maintenance costs presented in Tables 1 and 2, the following analysis evaluates the expected annual energy savings, operating costs, and simple payback period of the proposed residential PV–EV charging system.

Since these maintenance activities do not necessarily occur simultaneously or with the same annual frequency, Table 2 presents indicative cost ranges for individual interventions rather than a cumulative annual cost. For the simplified payback analysis, these recurring and occasional expenditures are represented by an annualized maintenance allowance of 100 USD/year, which provides a first-order estimate of the expected maintenance burden over the project lifetime. Table 3 summarizes the main energy and economic indicators for the proposed system.

Table 3. Annual energy consumption and economic results for EV charging and PV integration

Parameter	Value
Annual EV driving distance	22,000 km/year
EV energy consumption	0.20 kWh/km
Annual EV energy demand	4,400 kWh/year
Grid electricity tariff (Ecuador)	0.099 USD/kWh
Annual EV charging cost (grid only)	435.6 USD/year
PV system rated power	6 kW
Annual PV energy production	8,400 kWh/year
EV demand covered by PV system	70%
Gross annual EV charging savings	304.9 USD/year
Annualized PV maintenance allowance	100 USD/year
Net EV charging savings	205 USD/year
Additional household electricity savings	350 USD/year
Total net annual savings	555 USD/year

The economic indicator adopted in this preliminary assessment is the simple payback period, calculated as the ratio between the initial investment and the estimated annual net savings. Accordingly, the results should be interpreted as a first-order economic comparison among the three scenarios rather than as a complete life-cycle financial analysis. Factors such as discount rate, electricity-price escalation, PV degradation, equipment replacement, financing costs, and residual value are not explicitly included.

As shown in Table 4, the economic results reveal a strong dependence on the initial investment cost under the electricity tariff considered for Ecuador. Using the estimated total net annual savings of 555 USD/year, the simple payback periods are approximately 13.7, 21.3, and 31.9 years for the economy, standard, and professional scenarios, respectively. Consequently, the economy configuration provides the most favorable economic result, whereas the higher initial costs of the Standard and Professional configurations substantially extend the investment-recovery period.

Table 4. Estimated payback period for different investment scenarios

Scenario	Investment (USD)	Savings (USD/year)	Payback (years)
Economy	7,575	555	13.7
Standard	11,800	555	21.3
Professional	17,700	555	31.9

These results also show that technical feasibility does not necessarily imply short-term economic attractiveness. Under the assumptions adopted in this study, the relatively low residential electricity tariff limits the monetary value of the energy displaced by the PV system. The economic performance can therefore be expected to depend strongly on local electricity prices, PV installation costs, annual vehicle utilization, the fraction of PV energy effectively used for EV charging and household consumption, and the service life of the main conversion equipment.

Figure 4 compares the accumulated cost over time of a grid-only strategy against three PV-integrated EV charging configurations. The grid-only curve increases linearly as it reflects continuous energy purchases. A second curve is included to illustrate a sensitivity case in which the electricity price is doubled. Figure 4 complements the tabulated results by illustrating how the initial PV-system investment is progressively compensated by the reduction in grid-energy purchases. The economy scenario reaches the break-even condition first because its lower initial investment produces the largest ratio of annual savings to capital cost. In contrast, the additional capital expenditure associated with the standard and professional scenarios is not accompanied

by a proportional increase in the annual monetary savings, which explains their substantially longer payback periods.

A sensitivity case with a higher electricity tariff is also included in Figure 4. This comparison illustrates an important characteristic of residential PV–EV integration: as the cost of grid-supplied energy increases, the economic value of locally generated PV energy increases accordingly and the investment-recovery period decreases. Therefore, the economic conclusions obtained here are specific to the tariff and cost assumptions adopted in the study and should not be generalized directly to other electricity markets.

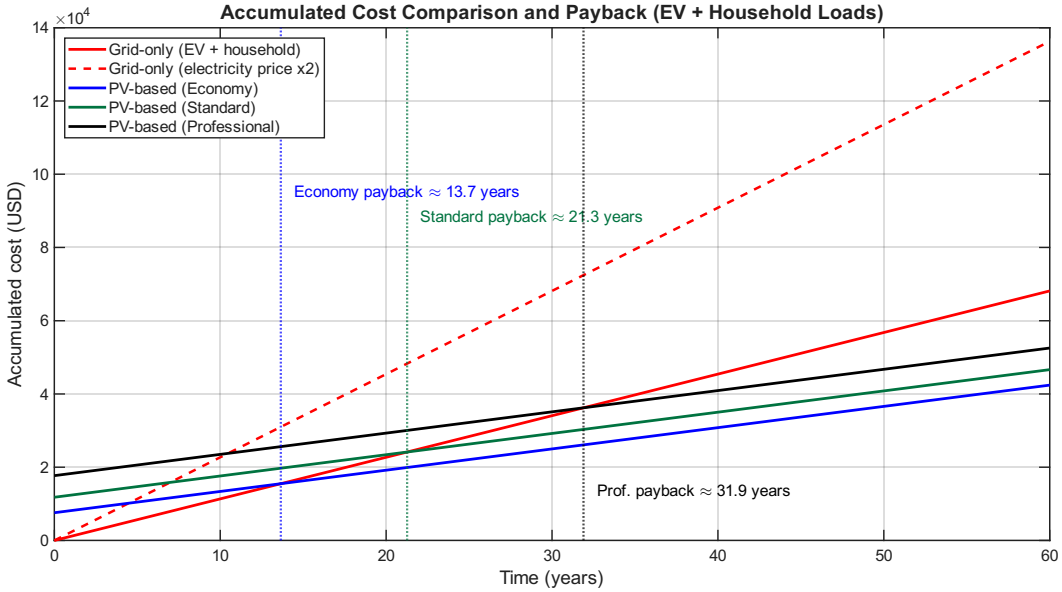


Figure 4. Accumulated cost comparison and payback

3. RESULTS AND DISCUSSION

This section reports ATPDraw/ATP–EMTP results for; i) PV subsystem evaluation, ii) inverter modulation and harmonic behavior, and iii) single-phase P–Q regulation performance. Results include characteristic curves and key electrical variables for analyzing the system's grid-integrated performance.

In addition to verifying the operation of the individual subsystems, the results are discussed in terms of their physical interpretation and their interaction within the complete PV–EV charging architecture. Particular attention is given to the double-frequency power behavior inherent to single-phase grid interfaces and to the ability of the proposed integrated model to reproduce these dynamics.

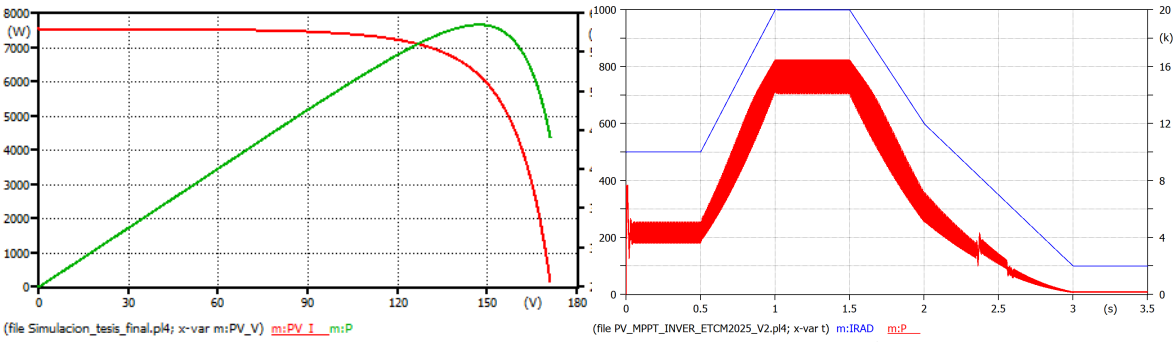
3.1. Modeling results of the photovoltaic system in ATPDraw

3.1.1. Photovoltaic array characteristics and irradiance response

Figure 5 summarizes the steady-state electrical behavior and the dynamic irradiance response of the implemented PV subsystem. Figure 5(a) shows the I–V and P–V characteristics under the selected irradiance and temperature conditions. The I–V curve exhibits the expected nonlinear profile with clearly defined short-circuit current and open-circuit voltage, while the P–V curve presents a single maximum power point (MPP). This confirms that the PV model reproduces the fundamental conversion characteristics required for subsequent MPPT evaluation.

Figure 5(b) illustrates the imposed irradiance profile and the corresponding power response of the PV subsystem. The irradiance is initially maintained at approximately 500 W/m^2 and is subsequently increased toward 1000 W/m^2. During the initial steady irradiance interval, the PV system delivers an average power of approximately 5.62 kW. As the irradiance increases, the available PV power also increases, while the transient evolution of the generated power reflects the combined dynamics of the PV array and the associated conversion and MPPT stages. This response confirms that the implemented model reproduces not only the expected dependence of available PV power on irradiance but also the dynamic behavior that the downstream grid-side controller must accommodate.

The location of the maximum in the P–V characteristic is particularly relevant to the complete charging system because it defines the operating point that must be imposed by the MPPT-controlled DC–DC converter. As the irradiance changes, the available PV power changes accordingly, requiring the DC–DC stage and the grid-side converter to accommodate the resulting power variation. Therefore, the response in Figure 5(b) is not only an evaluation of the PV model but also represents an external disturbance applied to the subsequent power-regulation stages. This behavior is consistent with established PV models and MPPT operation [24]–[26]; in the present work, however, the PV subsystem is evaluated as part of the complete grid-connected charging chain rather than as an isolated MPPT stage.

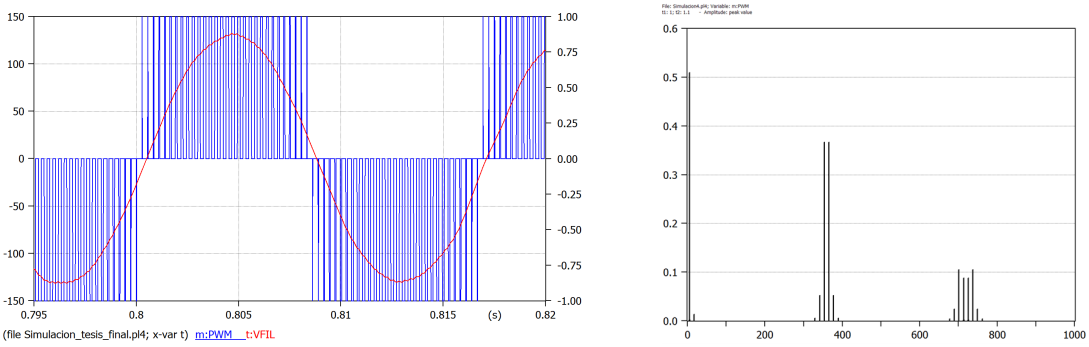


(a) (b)

Figure 5. Electrical characteristics and irradiance response of the PV system; (a) PV array I–V and P–V curves and (b) solar irradiance (blue) and generated power

3.2. Comparison of sinusoidal pulse width modulation, inverter output voltage, and harmonic spectrum

Figure 6 illustrates the voltage synthesis process of the single-phase inverter and the associated harmonic content of the SPWM modulation. In Figure 6(a), the SPWM switching signal and the low-pass filtered inverter output voltage are shown. The filtering stage effectively reconstructs a quasi-sinusoidal voltage waveform from the high-frequency switching pattern, whose fundamental component accurately follows the sinusoidal reference imposed by the SPWM strategy. This confirms the correct operation of the modulation, switching devices, and output filter in producing the desired AC voltage. The harmonic spectrum in Figure 6(b) shows the expected concentration of switching-related components at frequencies well above the fundamental component, providing the basis for their attenuation by the output filter. However, since this spectrum represents the PWM switching signal, it illustrates the frequency distribution produced by the modulation strategy rather than providing a quantitative measurement of the THD of the filtered grid-side voltage.

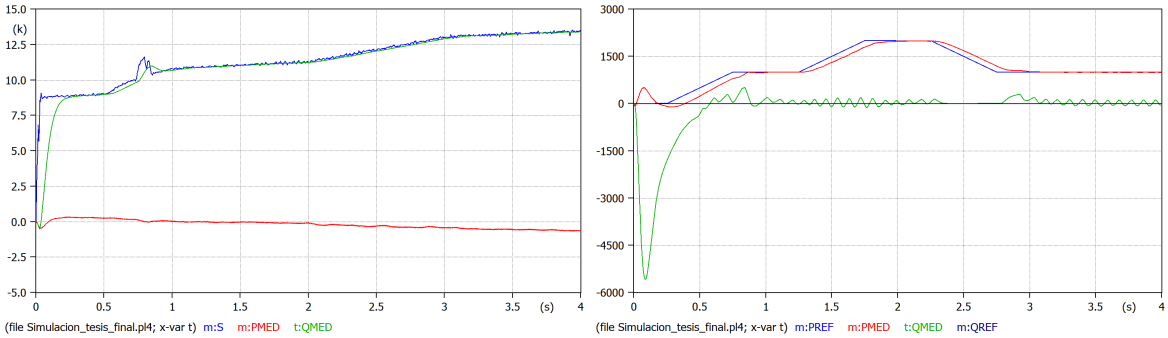


(a) (b)

Figure 6. SPWM waveform generation and corresponding harmonic content for the single-phase inverter; (a) SPWM signal and filtered inverter output voltage and (b) harmonic spectrum of the SPWM signal

3.3. Apparent, active, and reactive power

Figure 7 compares the system power behavior under uncontrolled and controlled operating conditions. In Figure 7(a), the apparent power S, active power P, and reactive power Q are shown without power control. In this case, power exchange is governed solely by the voltage magnitude difference and the phase relationship between the inverter and the grid. As a consequence, reactive power dominates due to the higher inverter voltage magnitude, while the active power remains close to zero, resulting in an apparent power that is largely defined by the reactive component. Figure 7(b) presents the controlled responses of active and reactive power together with their reference signals.



(a) (b)

Figure 7. Comparison of apparent (S), active (P), and reactive (Q) power under uncontrolled and controlled operating conditions; (a) apparent, active, and reactive power without control and (b) controlled active and reactive power with reference signals

The active-power reference is varied during the simulation from 0 to 1 kW, subsequently increased to 2 kW, and finally reduced to 1 kW in order to evaluate the dynamic behavior of the complete system over different operating points. After completion of the corresponding reference ramps, the measured active power enters and remains within a $\pm 2\%$ band around its reference in approximately 0.24 s, 0.18 s, and 0.24 s, respectively. In representative steady-state intervals, the average measured powers are approximately 996 W and 1988 W for reference values of 1 kW and 2 kW, corresponding to average tracking errors below 0.7%. These results demonstrate that the controller regulates the average active-power transfer effectively during both increasing and decreasing power commands.

The reactive-power reference is maintained close to zero throughout the test. Although the measured reactive power exhibits transient excursions and residual oscillations following changes in active power, its average value remains small compared with the transferred active power. For example, during the final 1 kW operating interval, the average measured active power and reactive-power estimate are approximately 996 W and 21 var, respectively. This indicates that the controller substantially reduces the reactive-power exchange while maintaining the commanded active-power transfer.

The remaining oscillatory behavior must be interpreted in the context of single-phase power conversion. For sinusoidal voltage and current, instantaneous power inherently contains a component at twice the grid frequency, unlike a balanced three-phase system where the corresponding oscillatory components cancel among phases. This characteristic complicates the extraction and regulation of average active and reactive power and motivates the use of synchronization, filtering, and dedicated power-control strategies in single-phase grid-connected converters [8], [9]. In the present implementation, the measured power signals are processed by the control structure; consequently, the oscillations observed in Figure 7(b) should not be interpreted directly as the unfiltered twice-grid-frequency instantaneous power component.

More advanced single-phase converter controls reported in the literature employ synchronous-reference-frame techniques, adaptive filters, and dedicated second-harmonic suppression methods to further reduce power oscillations [10], [11]. The objective of the present work is not to propose a new power-control algorithm, but to demonstrate that a comparatively simple PI–PLL structure can provide satisfactory average P–Q regulation when integrated with the complete PV–EV conversion chain in ATP–EMTP. The obtained sub-0.7% steady-state active-power tracking error and low average reactive-power exchange support this system-level objective.

4. CONCLUSION

This work developed a unified circuit-level ATP–EMTP/ATPDraw model of a PV-integrated EV charging system for single-phase electrical grids. The model combines PV generation, MPPT-controlled DC–DC conversion, SPWM inverter operation, output filtering, PLL-based synchronization, and coordinated active- and reactive-power regulation within the same simulation framework. The main contribution is therefore the integrated representation of the complete conversion and control chain rather than the proposal of a new converter topology or control algorithm.

Simulation results show stable operation under variable irradiance and effective regulation of average grid power. For active-power references between 1 and 2 kW, representative steady-state tracking errors remained below 0.7%, while the final 1 kW operating interval exhibited an average active power of approximately 996 W and an average reactive-power estimate of approximately 21 var. The results also reproduce the dynamic characteristics associated with single-phase power conversion and demonstrate that the PI–PLL control structure can maintain coordinated average P–Q regulation under the investigated operating conditions.

The technical–economic assessment further indicates that technical feasibility does not necessarily imply short-term economic attractiveness. Under the assumptions adopted for Ecuador, the estimated simple payback periods are approximately 13.7, 21.3, and 31.9 years for the economy, standard, and professional configurations, respectively, highlighting the strong influence of initial investment and local electricity tariffs on economic viability.

The present study is limited to circuit-level simulation and a first-order economic assessment; experimental validation, formal grid-code compliance testing, and a complete life-cycle financial analysis were not performed. Future work should therefore include hardware or hardware-in-the-loop validation, dedicated mitigation of single-phase double-frequency power oscillations, and evaluation of advanced energy management and bidirectional grid-support strategies.

ACKNOWLEDGMENTS

The authors gratefully acknowledge Universidad Politécnica Salesiana, Cuenca Campus, and particularly the Energy Research Group (GIE), for the institutional and academic support provided during the development of this research.

FUNDING INFORMATION

Authors state no funding involved.

AUTHOR CONTRIBUTIONS STATEMENT

This journal uses the Contributor Roles Taxonomy (CRediT) to recognize individual author contributions, reduce authorship disputes, and facilitate collaboration.

Name of Author	C	M	So	Va	Fo	I	R	D	O	E	Vi	Su	P	Fu
José Manuel Aller	✓	✓		✓	✓	✓			✓	✓		✓	✓	
Cristian Fernando León Zhagñay		✓	✓		✓	✓			✓		✓			
Bruno Vinicio Ortiz Cárdenas			✓	✓		✓		✓	✓		✓			

C : **C**onceptualization
M : **M**ethodology
So : **So**ftware
Va : **Va**lidation
Fo : **Fo**rmal Analysis
I : **I**nvestigation
R : **R**esources
D : **D**ata Curation
O : Writing - **O**riginal Draft
E : Writing - Review & **E**diting
Vi : **Vi**sualization
Su : **Su**pervision
P : **P**roject Administration
Fu : **Fu**nding Acquisition

CONFLICT OF INTEREST STATEMENT

Authors state no conflict of interest.

DATA AVAILABILITY

The authors confirm that the data supporting the findings of this study (ATPDraw model and MODELS Code) can be obtained from the corresponding author upon request at the email address: jaller@ups.edu.ec.

REFERENCES

[1] B. K. Sovacool, J. Axsen, and W. Kempton, "The Future Promise of Vehicle-to-Grid (V2G) Integration: A Sociotechnical Review and Research Agenda," *Annual Review of Environment and Resources*, vol. 42, pp. 377 – 406, 2017, doi: 10.1146/annurev-environ-030117-020220.

[2] G. Vishnu, D. Kaliyaperumal, R. Jayaprakash, A. Karthick, V. K. Chinnaiyan, and A. Ghosh, "Review of Challenges and Opportunities in the Integration of Electric Vehicles to the Grid," *World Electric Vehicle Journal*, vol. 14, no. 9, 2023, doi: 10.3390/wevj14090259.

[3] R. Rana, T. S. Saggu, S. S. Letha, and F. I. Bakhsh, "V2G based bidirectional EV charger topologies and its control techniques: a review," *Discover Applied Sciences*, vol. 6, no. 11, 2024, doi: 10.1007/s42452-024-06297-z.

[4] K. Zeb *et al.*, "A review on recent advances and future trends of transformerless inverter structures for single-phase grid-connected photovoltaic systems," *Energies*, vol. 11, no. 8, 2018, doi: 10.3390/en11081968.

[5] M. K. Hossain, P. Chowdhury, I. Nowshin, M. R. Islam, A. Al-Hysam, and O. Farrok, "Grid-connected inverter for photovoltaic energy harvesting: Advances in topologies and control techniques," *Energy Conversion and Management: X*, vol. 29, 2026, doi: 10.1016/j.ecmx.2025.101422.

[6] F. B. Grigoletto, "Five-Level Transformerless Inverter for Single-Phase Solar Photovoltaic Applications," *IEEE Journal of Emerging and Selected Topics in Power Electronics*, vol. 8, no. 4, pp. 3411 – 3422, 2020, doi: 10.1109/JESTPE.2019.2891937.

[7] L. Ma, H. Xu, A. Q. Huang, X. Wang, and J. Zou, "Single-phase hybrid-H6 transformerless PV grid-tied inverter," *IET Power Electronics*, vol. 11, no. 15, pp. 2440 – 2449, 2018, doi: 10.1049/iet-pel.2018.5009.

[8] Y. Wang, J.-W. Yang, W.-J. Kim, T.-H. Kwon, T. Lee, and S.-J. Park, "Second Harmonic Current Suppression and Dynamic Response Improvement for V2G System," *IEEE Transactions on Power Electronics*, vol. 38, no. 8, pp. 9566 – 9580, 2023, doi: 10.1109/TPEL.2023.3275575.

[9] H. Zhou, L. He, Z. Yang, and Z. Lin, "Virtual Fractional-Order-Inductor Based Second Harmonic Current Suppression Method," *IEEE Transactions on Industrial Electronics*, vol. 71, no. 8, pp. 8949 – 8959, 2024, doi: 10.1109/TIE.2023.3314915.

[10] S. Somkun, S. Srita, T. Kaewchum, A. Pannawan, C. Saeseiw, and P. Pachanapan, "Adaptive Notch Filters for Bus Voltage Control and Capacitance Degradation Prognostic of Single-Phase Grid-Connected Inverter," *IEEE Transactions on Industrial Electronics*, vol. 70, no. 12, pp. 12190 – 12200, 2023, doi: 10.1109/TIE.2023.3237904.

[11] A. S. Al-Khayyat, A. Al-Safi, and M. J. Hameed, "Single-phase grid-connected power control in dq synchronous reference frame with space vector modulation using FPGA," *Indonesian Journal of Electrical Engineering and Computer Science*, vol. 30, no. 1, pp. 57–69, 2023, doi: 10.11591/ijeecs.v30.i1.pp57-69.

[12] H. K. Høidalen, *ATPDraw for Windows—User's Manual*, NTNU, Department of Electric Power Engineering, Trondheim, Norway, 2014.

[13] L. Dubé, MODELS in ATP: Language Manual, *European EMTP-ATP Users Group e.V. News*, vol. 2, no. 1, pp. 12–24, 1996.

[14] B. H. Yong, and V. K. Ramachandaramurthy, "Harmonic mitigation of grid connected 5MW solar PV using LCL Filter," in *3rd IET International Conference on Clean Energy and Technology (CEAT) 2014*, 2014, doi: 10.1049/cp.2014.1458.

[15] K.-J. Lee, N.-J. Park, R.-Y. Kim, D.-H. Ha, and D.-S. Hyun, "Design of an LCL filter employing a symmetric geometry and its control in grid-connected inverter applications," in *2008 IEEE Power Electronics Specialists Conference*, pp. 963 – 966, 2008, doi: 10.1109/PESC.2008.4592054.

[16] K. M. El-Naggar, "A dynamic filter for removal DC - offset in current and voltage waveforms," *World Academy of Science, Engineering and Technology*, vol. 50, pp. 384–388, 2011.

[17] J. Aller and G. Orellana, "Modeling a PV System Connected to the Grid using Optimal Direct Power Control (ODPC) with ATP-EMTP and ATPDraw," in *2025 IEEE Nineth Ecuador Technical Chapters Meeting (ETCM)*, pp. 1-6, 2025, doi: 10.1109/ETCM67548.2025.11304498.

[18] E. Kabalci, "SiC-Based Single-Phase Transformerless Grid-Tied Inverter with Enhanced PLL Control," in *Proceedings - 2026 8th Global Power, Energy and Communication Conference, GPECOM 2026*, pp. 57 – 64, 2026, doi: 10.1109/GPECOM70462.2026.11578420.

[19] Y. Ding, M. Mao, and L. Chang, "Conservative power theory and its applications in modern smart grid: Review and prospect," *Applied Energy*, vol. 303, 2021, doi: 10.1016/j.apenergy.2021.117617.

[20] M. A. S. T. Ireshika and P. Kepplinger, "IEC 61851 compliant demand side management algorithm for electric vehicle charging: a MILP based decentralized approach," in *13th Mediterranean Conference on Power Generation, Transmission, Distribution and Energy Conversion (MEDPOWER 2022)*, 2022, pp. 146-152, doi: 10.1049/icp.2022.3317.

[21] S. Nayak, P. Daigavane, A. A. K. Majhi, S. Parida, M. P. Behera, and S. Mohanty, "Single-Phase Bidirectional PEV Charger for Different Power Factor Conditions," in *2025 IEEE 1st International Conference on Recent Trends in Computing and Smart Mobility, RCSM 2025*, 2025, pp. 1-6, doi: 10.1109/RCSM67767.2025.11506695.

[22] IEEE, "IEEE Application Guide for IEEE Std 1547™-2018, IEEE Standard for Interconnection and Interoperability of Distributed Energy Resources with Associated Electric Power Systems Interfaces," *IEEE Std 1547.2-2023 (Revision of IEEE Std 1547.2-2008)*, pp. 1-291, 2024, doi: 10.1109/IEEESTD.2024.10534228.

[23] IEEE, "IEEE Standard for Technical Specifications of a DC Quick and Bidirectional Charger for Use with Electric Vehicles - Redline," *IEEE Std 2030.1.1-2021 (Revision of IEEE Std 2030.1.1-2015) - Redline*, pp. 1-263, 2022, doi: 10.1109/IEEESTD.2022.9760299.

[24] N. Kumar, I. Hussain, B. Singh, and B. K. Panigrahi, "Rapid MPPT for Uniformly and Partial Shaded PV System by Using JayaDE Algorithm in Highly Fluctuating Atmospheric Conditions," *IEEE Transactions on Industrial Informatics*, vol. 13, no. 5, pp. 2406–2416, 2017, doi: 10.1109/TII.2017.2700327.

[25] V. Bhardwaj and P. Gaur, "A Fuzzy-Based Buck-Boost Photovoltaic Inverter for Voltage Stabilization During Mismatched Environmental Conditions," in *Recent Advances in Power Electronics and Drives: Select Proceedings of EPREC 2021*, vol. 852, pp. 451–466, 2022, doi: 10.1007/978-981-16-9239-0_34.

[26] C. Balaji, O. Hemakesavulu, A. D. Savio, B. Vinothkumar, S. Sakthi, and P. Sivaperumal, "A Trasformerless Buck-Boost Converter as Maximum Power Point Tracker for Battery Charging," in *Proceedings of International Conference on Power Electronics and Renewable Energy Systems*, vol. 795, pp. 237 – 246, 2022, doi: 10.1007/978-981-16-4943-1_22.

BIOGRAPHIES OF AUTHORS



Dr. José Manuel Aller was born in Caracas, Venezuela, in 1958. He received the B.Sc. degree in Electrical Engineering from the Universidad Simón Bolívar, Caracas, in 1980, the M.S. degree in Electrical Engineering from the Universidad Central de Venezuela, Caracas, in 1982, and the Ph.D. degree in Industrial Engineering from the Universidad Politécnica de Madrid, Spain, in 1993. He has been a lecturer at the Universidad Simón Bolívar for 36 years. From 2001 to 2005, he served as the general secretary of the Universidad Simón Bolívar. He was also a visiting professor at the Georgia Institute of Technology, Atlanta, GA, USA, in 2000 and 2007. Since 2016, he has been a full-time professor of Electrical Machines and Electromagnetism in the Department of Electrical Engineering at the Universidad Politécnica Salesiana, Cuenca, Ecuador. He has published over 120 papers in his field. His research interests include space-vector applications, electrical machine control, power electronics, and the monitoring of electrical machines. He can be contacted at email: jaller@ups.edu.ec.



Cristian Fernando León Zhagñay was born in Azogues, Ecuador, in 2002, he received the B.Sc. degree in Electrical Engineering from Universidad Politécnica Salesiana (ABET accredited) in 2026. He completed his professional internship at Empresa Eléctrica de Azogues, where he gained experience in power distribution infrastructure and maintenance. In 2025, he completed his undergraduate thesis entitled "Design of Electric Vehicle Chargers with Photovoltaic Systems and Grid Integration." His research interests include power electronics, electric power systems, electric mobility, and renewable energy technologies. He can be contacted at email: cleonz1@est.ups.edu.ec.



Bruno Vinicio Ortiz Cárdenas was born in Cuenca, Ecuador, in 2003, he received the B.Sc. degree in Electrical Engineering from Universidad Politécnica Salesiana (ABET accredited) in 2026. He completed his professional internship at Continental Tire Andina, where he gained experience in electrical systems, industrial automation, and maintenance. In 2025, he developed his final degree project entitled "Design of Electric Vehicle Chargers with Photovoltaic Systems and Integration into the Electrical Grid." His research interests include power electronics, electric power systems, electric mobility, and renewable energy. He can be contacted at email: ortizc1@est.ups.edu.ec.